AIAA JOURNAL
Vol. 40, No. 8, August 2002

Viscoelastic Analysis of Multiphase Composites Using the Generalized Method of Cells

Carlos E. Orozco*
University of North Carolina, Charlotte, North Carolina 28223
and
Marek-Jerzy Pindera†
University of Virginia, Charlottesville, Virginia 22903

A computationally efficient formulation of the generalized method of cells is extended to deal with linear viscoelastic behavior. The resulting viscoelastic capability is utilized to calculate the viscoelastic responses of fiber-reinforced unidirectional composites with polymeric matrices. A multi-axial hereditary viscoelastic model is used as the theoretical basis of the formulation. The creep compliances of composites with different fiber shapes and microstructure architectures are analyzed and compared. To estimate accurately the influence of fiber shape, high-resolution cell models (with up to 10,000 subcells) of the composites are used in the numerical experiments. Results show that differences in creep response due to differences in fiber shape are not dramatic but that significant differences exist for the cases with different fiber arrangements.

I. Introduction

DEMAND for light, strong, and durable materials such as composites is likely to increase in the near future as the aerospace industry strives for developing a new generation of air and space vehicles. On the other hand, powerful computational and analytical techniques allow for the modeling of complex materials with a degree of detail not possible before. Furthermore, this computational power makes the creation of a complete analysis and design capability for aerospace vehicles a distinct possibility in the 21st century. Detailed micromechanical analysis of multiphase composites are likely to be an important part of this general analysis and design capability. As a matter of fact, the numerical capability developed in connection with the present study has been implemented in the commercial aircraft design and analysis code Hypersizer® (Collier Research and Development Co.). This micromechanical analysis capability incorporates a viscoelastic model into the widely utilized generalized method of cells (GMC).[1] The GMC has been utilized successfully during the past 10 years to model composites under a variety of thermomechanical conditions.[2] The precursor of GMC, called simply method of cells, utilized a very simple discretization scheme (with just four subcells).[3] This method proved useful in modeling simple (mainly two-phase) unidirectional composites. The method was subsequently generalized to allow the modeling of composites with an arbitrary number of subcells. In its original version, however, the GMC remained computationally limited to about 500 subcells (for inelastic analysis). In its present form, GMC allows calculations with more than 10,000 subcells. This was made possible by two independent developments. The first development involved a reformulation of the GMC equations that effectively reduces the number of independent unknowns, thereby greatly reducing the computational and storage requirements of the method. This work was done by Pindera and Bednarcyk.[4] This reformulated version of GMC is currently available in the NASA John H. Glenn Research Center computer code MAC.[5] The second development takes advantage of the sparsity of the matrices in GMC to reduce the computational and storage requirements of the method. This results in a computationally efficient sparse implementation of GMC. Sparse formulations of GMC have been described and utilized in Refs. 6 and 7, where they have been applied to elasticity and plasticity problems, respectively. The present study extends the applicability of this computationally efficient sparse formulation of GMC to viscoelastic problems. Viscoelastic models have been used in conjunction with GMC in Ref. 8 and most recently in Ref. 9. In Ref. 8, the original method of cells (with four subcells) in conjunction with the correspondence principle and Laplace transforms was used to model polymeric matrix composites. In Ref. 9, a finite-deformation viscoelastic model is incorporated into the three-dimensional version of GMC and used to study the behavior of short-fiber composites. In the present study, a simpler multi-axial viscoelastic hereditary model developed in Ref. 10 is used as the theoretical framework. The resulting GMC formulation is suitable for modeling the viscoelastic response of unidirectional composites with a high degree of detail in a computationally efficient manner. A simple integration scheme based on the analytical solution of the governing differential equation of the hereditary model is also developed and presented. The hereditary model formulation is illustrated in the context of a standard three-element solid model (Fig. 1a).

Received 25 May 2000; revision received 30 November 2001; accepted for publication 18 March 2002.

*Associate Professor, Department of Engineering Technology. Member AIAA.
†Professor, Department of Civil Engineering.

II. GMC

The GMC[1,3] is a micromechanics model that has proven to be effective in modeling the elastic and inelastic behavior of fiber-reinforced unidirectional composites.[2] The method starts by dividing the cross section of the composite into unit cells that correspond to representative volume elements (RVEs). The unit cells or RVEs are in turn divided into subdomains called subcells. Figure 2 shows a unit cell with the corresponding subcells and the associated nomenclature. The reinforcing fibers are assumed to extend in the x_1 direction. When started with the material properties of the constituents and the corresponding material constitutive models, GMC uses traction and displacement continuity conditions, together with a stress averaging procedure, to obtain the effective (or average) properties and the effective behavior of the composite. GMC is, therefore, a volume averaging method.

Models of unidirectional composites using GMC satisfy traction and displacement continuity in an average sense.[1] The explicit form of the traction and displacement continuity conditions can be found in Ref. 1, 6, or 7. The displacement continuity conditions can be written compactly in matrix form as

$$\boldsymbol{A}_G \boldsymbol{\varepsilon}_N = \boldsymbol{J}\bar{\boldsymbol{\varepsilon}} \tag{1}$$

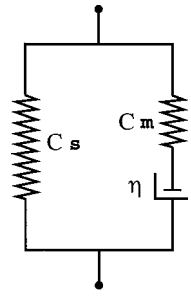

Fig. 1a Standard linear three-element solid model.

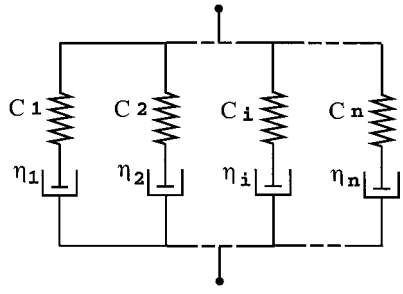

Fig. 1b Multi-element model with Maxwell elements in parallel.

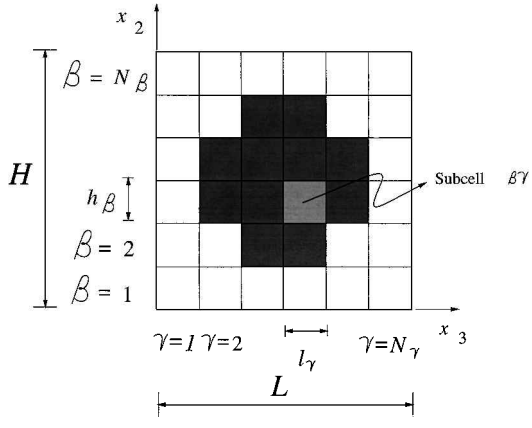

Fig. 2 Repeating unit cell with subcells and nomenclature.

where $\varepsilon_N \equiv \{\varepsilon^{(1,1)}, \varepsilon^{(1,2)}, \ldots, \varepsilon^{(N_\beta, N_\gamma)}\}^T$ contains $N_\beta N_\gamma$ vectors of subcell strains $\varepsilon^{(\beta\gamma)}$ and $\bar{\varepsilon} \equiv \{\bar{\varepsilon}_{11}, \bar{\varepsilon}_{22}, \bar{\varepsilon}_{33}, 2\bar{\varepsilon}_{23}, 2\bar{\varepsilon}_{13}, 2\bar{\varepsilon}_{12}\}^T$ contains the effective strains. The matrices $\boldsymbol{A}_G$ and $\boldsymbol{J}$ contain information about subcell and cell geometry. Their entries are (h_β and l_γ) $h_\beta l_\gamma$ products, (H and L) HL products, and 1s and 0s (Fig. 2).

On the other hand, for a wide variety of material behavior, the constitutive relationships can be written as

$$\boldsymbol{\sigma} = \boldsymbol{C}\left(\varepsilon - \varepsilon^* - \varepsilon_T\right) \tag{2}$$

where $\boldsymbol{C}$ is the stiffness matrix of the material, ε_T is the thermal strain, and ε^* is an inelastic strain, for example, plastic or viscoplastic. It is shown in the next section that this constitutive relationship is also valid for many spring–dashpot viscoelastic models provided ε^* is taken as a modified viscous strain $\hat{\varepsilon}_\eta$. For all of these models, GMCs traction continuity conditions (Ref. 1, 6, or 7) can be written as

$$\boldsymbol{A}_M(\varepsilon_N - \hat{\varepsilon}_{N\eta} - \varepsilon_{NT}) = \boldsymbol{0} \tag{3}$$

where $\hat{\varepsilon}_{N\eta}$ and ε_T are the (modified) viscous and thermal strains of all subcells. Equations (1) and (3) can be written compactly as

$$\boldsymbol{A}\varepsilon_N = \boldsymbol{K}\bar{\varepsilon} + \boldsymbol{A}^I\hat{\varepsilon}_{N\eta} + \boldsymbol{A}^I\varepsilon_{NT} \tag{4}$$

where

$$\boldsymbol{A} \equiv \begin{bmatrix} \boldsymbol{A}_G \\ \boldsymbol{A}_M \end{bmatrix} \tag{5}$$

$$\boldsymbol{A}^I \equiv \begin{bmatrix} \boldsymbol{0} \\ \boldsymbol{A}_M \end{bmatrix} \tag{6}$$

$$\boldsymbol{K} \equiv \begin{bmatrix} \boldsymbol{J} \\ \boldsymbol{0} \end{bmatrix} \tag{7}$$

Solving for the total strain in Eq. (4), one gets

$$\varepsilon_N = \boldsymbol{A}^{-1}\boldsymbol{K}\bar{\varepsilon} + \boldsymbol{A}^{-1}\boldsymbol{A}^I\hat{\varepsilon}_{N\eta} + \boldsymbol{A}^{-1}\boldsymbol{A}^I\varepsilon_{NT} \tag{8}$$

or

$$\varepsilon_N = \boldsymbol{A}_s\bar{\varepsilon} + \boldsymbol{A}_s^I\hat{\varepsilon}_{N\eta} + \boldsymbol{A}_s^I\varepsilon_{NT} \tag{9}$$

where

$$\boldsymbol{A}_s \equiv \boldsymbol{A}^{-1}\boldsymbol{K} \tag{10}$$

$$\boldsymbol{A}_s^I \equiv \boldsymbol{A}^{-1}\boldsymbol{A}^I \tag{11}$$

The subcell stresses can now be computed as

$$\boldsymbol{\sigma}^{(\beta\gamma)} = \boldsymbol{C}^{(\beta\gamma)}\left[\boldsymbol{A}_s^{(\beta\gamma)}\bar{\varepsilon} + \boldsymbol{A}_s^{I(\beta\gamma)}\hat{\varepsilon}_{N\eta} + \boldsymbol{A}_s^{I(\beta\gamma)}\varepsilon_{NT} - \hat{\varepsilon}_\eta^{(\beta\gamma)} - \varepsilon_T^{(\beta\gamma)}\right] \tag{12}$$

where $\boldsymbol{C}^{(\beta\gamma)}$ is the stiffness matrix corresponding to the material in subcell $(\beta\gamma)$, and $\boldsymbol{A}_s^{(\beta\gamma)}$ and $\boldsymbol{A}_s^{I(\beta\gamma)}$ are submatrices of $\boldsymbol{A}_s$ and $\boldsymbol{A}_s^I$ corresponding to subcell $(\beta\gamma)$.

Applying now the definition of average stress to Eq. (12), one obtains

$$\begin{aligned}\bar{\boldsymbol{\sigma}} = {} & \frac{1}{HL}\sum_\beta\sum_\gamma h_\beta h_\gamma \boldsymbol{C}^{(\beta\gamma)}\boldsymbol{A}_s^{(\beta\gamma)}\bar{\varepsilon} \\ & + \frac{1}{HL}\sum_\beta\sum_\gamma \left(h_\beta h_\gamma \boldsymbol{C}^{(\beta\gamma)}\boldsymbol{A}_s^{I(\beta\gamma)}\hat{\varepsilon}_{N\eta} - \hat{\varepsilon}_\eta^{(\beta\gamma)}\right) \\ & + \frac{1}{HL}\sum_\beta\sum_\gamma \left(h_\beta h_\gamma \boldsymbol{C}^{(\beta\gamma)}\boldsymbol{A}_s^{I(\beta\gamma)}\varepsilon_{NT} - \varepsilon_T^{(\beta\gamma)}\right)\end{aligned} \tag{13}$$

On the other hand, the effective average stress can be written as

$$\bar{\boldsymbol{\sigma}} = \bar{\boldsymbol{C}}(\bar{\varepsilon} - \bar{\hat{\varepsilon}}_\eta - \bar{\varepsilon}_T) \tag{14}$$

If the effective stiffness matrix is defined as

$$\bar{\boldsymbol{C}} = \frac{1}{HL}\sum_\beta\sum_\gamma h_\beta h_\gamma \boldsymbol{C}^{(\beta\gamma)}\boldsymbol{A}_s^{(\beta\gamma)} \tag{15}$$

Equation (13) can be written as

$$\begin{aligned}\bar{\boldsymbol{\sigma}} = \bar{\boldsymbol{C}}\Bigg[& \bar{\varepsilon} + \boldsymbol{C}^{-1}\frac{1}{HL}\sum_\beta\sum_\gamma \left(h_\beta h_\gamma \boldsymbol{C}^{(\beta\gamma)}\boldsymbol{A}_s^{I(\beta\gamma)}\hat{\varepsilon}_{N\eta} - \hat{\varepsilon}_\eta^{(\beta\gamma)}\right) \\ & + \boldsymbol{C}^{-1}\frac{1}{HL}\sum_\beta\sum_\gamma \left(h_\beta h_\gamma \boldsymbol{C}^{(\beta\gamma)}\boldsymbol{A}_s^{I(\beta\gamma)}\varepsilon_{NT} - \varepsilon_T^{(\beta\gamma)}\right)\Bigg]\end{aligned} \tag{16}$$

which on comparison with Eq. (14) suggests the following definition for the effective viscous and thermal strains:

$$\bar{\hat{\varepsilon}}_\eta = -\bar{\boldsymbol{C}}^{-1}\frac{1}{HL}\sum_\beta\sum_\gamma \left(h_\beta h_\gamma \boldsymbol{C}^{(\beta\gamma)}\boldsymbol{A}_s^{I(\beta\gamma)}\hat{\varepsilon}_{N\eta} - \varepsilon_\eta^{(\beta\gamma)}\right) \tag{17}$$

$$\bar{\varepsilon}_T = -\bar{\boldsymbol{C}}^{-1}\frac{1}{HL}\sum_\beta\sum_\gamma \left(h_\beta h_\gamma \boldsymbol{C}^{(\beta\gamma)}\boldsymbol{A}_s^{I(\beta\gamma)}\varepsilon_{NT} - \varepsilon_T^{(\beta\gamma)}\right) \tag{18}$$

III. Viscoelastic Hereditary Model

The basic hereditary viscoelastic relationships for a uniaxial case can be derived directly by applying equilibrium and compatibility to the three-element model shown in Fig. 1a. This model consists of a spring and a Maxwell element in parallel. C_s and C_m are the elastic moduli of the springs, and η is the damping coefficient of the dashpot in the Maxwell element. To obtain a multi-axial version of the hereditary model for the nonisothermal case, it is advantageous to use Gibbs free energy potential (see Ref. 10). The following discussion follows closely that of Ref. 10. When a multi-axial system analogous to that shown in Fig. 1a is referred to, Gibbs free energy potential takes the form

$$\Phi = -\tfrac{1}{2}\boldsymbol{\sigma}_s^T \boldsymbol{C}_s^{-1}\boldsymbol{\sigma}_s - \tfrac{1}{2}\boldsymbol{\sigma}_m^T \boldsymbol{C}_m^{-1}\boldsymbol{\sigma}_m - \tfrac{1}{2}\boldsymbol{\sigma}_m^T \boldsymbol{\varepsilon}_\eta - \alpha\,\mathrm{tr}(\boldsymbol{\sigma})(T - T_0) \tag{19}$$

where $\boldsymbol{C}_s$ is the elastic stiffness matrix of a homogeneous isotropic material with modulus of elasticity E_s and Poisson's ratio ν, $\boldsymbol{C}_m$ is the elastic stiffness matrix of a homogeneous isotropic material with modulus of elasticity E_m and Poisson's ratio ν, $\boldsymbol{\sigma}_s \equiv \{\sigma_{11}^s, \sigma_{22}^s, \sigma_{33}^s, \sigma_{23}^s, \sigma_{13}^s, \sigma_{12}^s\}^T$ are the stresses in the isolated spring element, $\boldsymbol{\sigma}_m \equiv \{\sigma_{11}^m, \sigma_{22}^m, \sigma_{33}^m, \sigma_{23}^m, \sigma_{13}^m, \sigma_{12}^m\}^T$ are the stresses in the Maxwell element, $\boldsymbol{\varepsilon}_\eta \equiv \{\varepsilon_{11}^\eta, \varepsilon_{22}^\eta, \varepsilon_{33}^\eta, 2\varepsilon_{23}^\eta, 2\varepsilon_{13}^\eta, 2\varepsilon_{12}^\eta\}^T$ are the strains in the viscous damper, α is the coefficient of thermal expansion of the material, and T_0 and T are the initial and current temperatures, respectively.

The strain rates corresponding to the spring and the Maxwell element can be obtained as

$$\dot{\boldsymbol{\varepsilon}}_s = \frac{\mathrm{d}}{\mathrm{d}t}\left(-\frac{\partial \Phi}{\partial \boldsymbol{\sigma}_s}\right) \tag{20}$$

$$\dot{\boldsymbol{\varepsilon}}_m = \frac{\mathrm{d}}{\mathrm{d}t}\left(-\frac{\partial \Phi}{\partial \boldsymbol{\sigma}_m}\right) \tag{21}$$

that is,

$$\dot{\boldsymbol{\varepsilon}}_s = \boldsymbol{C}_s^{-1}\dot{\boldsymbol{\sigma}}_s + \left[\frac{\partial \boldsymbol{C}_s^{-1}}{\partial T}\boldsymbol{\sigma}_s + \boldsymbol{\alpha} + \frac{\partial \boldsymbol{\alpha}}{\partial T}(T - T_0)\right]\dot{T} \tag{22}$$

$$\dot{\boldsymbol{\varepsilon}}_m = \boldsymbol{C}_m^{-1}\dot{\boldsymbol{\sigma}}_m + \left[\frac{\partial \boldsymbol{C}_m^{-1}}{\partial T}\boldsymbol{\sigma}_m + \boldsymbol{\alpha} + \frac{\partial \boldsymbol{\alpha}}{\partial T}(T - T_0)\right]\dot{T} + \dot{\boldsymbol{\varepsilon}}_\eta \tag{23}$$

where $\boldsymbol{\alpha} \equiv \{\alpha, \alpha, \alpha, 0, 0, 0\}^T$. Equations (22) and (23) can be written as

$$\dot{\boldsymbol{\varepsilon}}_s = \boldsymbol{C}_s^{-1}\dot{\boldsymbol{\sigma}}_s + \boldsymbol{\theta}_s\dot{T} \tag{24}$$

$$\dot{\boldsymbol{\varepsilon}}_m = \boldsymbol{C}_m^{-1}\dot{\boldsymbol{\sigma}}_m + \boldsymbol{\theta}_m\dot{T} + \dot{\boldsymbol{\varepsilon}}_\eta \tag{25}$$

where

$$\boldsymbol{\theta}_s \equiv \frac{\partial \boldsymbol{C}_s^{-1}}{\partial T}\boldsymbol{\sigma}_s + \boldsymbol{\alpha}_{\mathrm{lin}} \tag{26}$$

$$\boldsymbol{\theta}_m \equiv \frac{\partial \boldsymbol{C}_m^{-1}}{\partial T}\boldsymbol{\sigma}_m + \boldsymbol{\alpha}_{\mathrm{lin}} \tag{27}$$

with

$$\boldsymbol{\alpha}_{\mathrm{lin}} \equiv \boldsymbol{\alpha} + \frac{\partial \boldsymbol{\alpha}}{\partial T}(T - T_0)\dot{T} \tag{28}$$

In analogy with the model of Fig. 1a, the stress rates satisfy

$$\dot{\boldsymbol{\sigma}} = \dot{\boldsymbol{\sigma}}_m + \dot{\boldsymbol{\sigma}}_s \tag{29}$$

Also, using the constitutive relationships, we obtain

$$\dot{\boldsymbol{\sigma}}_s = \boldsymbol{C}_s(\dot{\boldsymbol{\varepsilon}}_s - \boldsymbol{\theta}_s\dot{T}) \tag{30}$$

$$\dot{\boldsymbol{\sigma}}_m = \boldsymbol{C}_m(\dot{\boldsymbol{\varepsilon}}_m - \dot{\boldsymbol{\varepsilon}}_\eta - \boldsymbol{\theta}_m\dot{T}) \tag{31}$$

On the other hand, from compatibility,

$$\dot{\boldsymbol{\varepsilon}} \equiv \dot{\boldsymbol{\varepsilon}}_s = \dot{\boldsymbol{\varepsilon}}_m \tag{32}$$

When Eqs. (29–32) are used, $\dot{\boldsymbol{\sigma}}$ can be written as

$$\dot{\boldsymbol{\sigma}} = \boldsymbol{C}_E\{\dot{\boldsymbol{\varepsilon}} - (E_m/E)\dot{\boldsymbol{\varepsilon}}_\eta - [(E_s/E)\boldsymbol{\theta}_s + (E_m/E)\boldsymbol{\theta}_m]\dot{T}\} \tag{33}$$

where

$$\boldsymbol{C}_E \equiv \boldsymbol{C}_s + \boldsymbol{C}_m \tag{34}$$

It is also assumed in Eq. (33) that

$$\boldsymbol{C}_s \equiv E_s\boldsymbol{N}, \qquad \boldsymbol{C}_m \equiv E_m\boldsymbol{N}, \qquad \boldsymbol{C}_E \equiv E\boldsymbol{N} \tag{35}$$

where $E \equiv E_s + E_m$ and $\boldsymbol{N}$ is a matrix that contains a common Poisson's ratio ν, 1s, and 0s. Assumption (35) relies on that the same value of Poisson's ratio can be be assumed for all multi-axial elements (springs and dashpots) in the viscoelastic model. It has been shown in Ref. 10 that this assumption produces responses that compare well with experimental results. Equation (33) can be written as

$$\dot{\boldsymbol{\sigma}} = \boldsymbol{C}_E(\dot{\boldsymbol{\varepsilon}} - \dot{\hat{\boldsymbol{\varepsilon}}}_\eta - \dot{\boldsymbol{\varepsilon}}_T) \tag{36}$$

where

$$\dot{\hat{\boldsymbol{\varepsilon}}}_\eta \equiv (E_m/E)\dot{\boldsymbol{\varepsilon}}_\eta \tag{37}$$

$$\dot{\boldsymbol{\varepsilon}}_T \equiv \hat{\boldsymbol{\alpha}}\dot{T} \tag{38}$$

with

$$\hat{\boldsymbol{\alpha}} \equiv (1/E)(E_s\boldsymbol{\theta}_s + E_m\boldsymbol{\theta}_m) \tag{39}$$

As pointed out in Sec. II, Eq. (36) allows the incorporation of the present viscoelastic model into the framework of a micromechanical method (such as GMC) much in the same way as inelastic, for example, plastic or viscoplastic, behavior is incorporated (for example, see Ref. 2). It is also possible to derive a similar expression for a multi-element model with an arbitrary number of Maxwell elements in parallel (Fig. 1b and the Appendix). Note, however, that these models ignore the nonlinear dependencies of Poisson's ratios pointed out in Refs. 11 and 12. Because the purpose of the present study is to demonstrate the applicability of the viscoelastic theory of Ref. 10 in conjunction with the GMC, the numerical results presented are limited to the three-element model shown in Fig. 1a.

When the present three-element model is used, a given homogeneous viscoelastic material will be characterized by a set of four material constants, E_m, E_s, η, and ν, at discrete temperature values.[10] It is useful then to find explicit expressions for the partial derivatives appearing in Eqs. (26) and (27) in terms of these material constants. This is done in the next paragraphs.

For a homogeneous isotropic material, $\boldsymbol{C}_s^{-1}$ corresponds to a compliance matrix given by

$$\boldsymbol{C}_s^{-1} = E_s^{-1}\boldsymbol{L} \tag{40}$$

where

$$\boldsymbol{L} \equiv \begin{bmatrix} 1 & -\nu & -\nu & 0 & 0 & 0 \\ -\nu & 1 & -\nu & 0 & 0 & 0 \\ -\nu & -\nu & 1 & 0 & 0 & 0 \\ 0 & 0 & 0 & 2+2\nu & 0 & 0 \\ 0 & 0 & 0 & 0 & 2+2\nu & 0 \\ 0 & 0 & 0 & 0 & 0 & 2+2\nu \end{bmatrix} \tag{41}$$

The partial derivative in Eq. (26) is then

$$\frac{\partial \boldsymbol{C}_s^{-1}}{\partial T} = -E_s^{-2}\frac{\partial E_s}{\partial T}\boldsymbol{L} + E_s^{-1}\frac{\partial \nu}{\partial T}\boldsymbol{L}_0 \tag{42}$$

where

$$\boldsymbol{L}_0 \equiv \begin{bmatrix} 0 & -1 & -1 & 0 & 0 & 0 \\ -1 & 0 & -1 & 0 & 0 & 0 \\ -1 & -1 & 0 & 0 & 0 & 0 \\ 0 & 0 & 0 & 2 & 0 & 0 \\ 0 & 0 & 0 & 0 & 2 & 0 \\ 0 & 0 & 0 & 0 & 0 & 2 \end{bmatrix} \tag{43}$$

The parameter $\boldsymbol{\theta}_s$ in Eq. (26) can now be expressed as

$$\boldsymbol{\theta}_s = \left(-E_s^{-2} \frac{\partial E_s}{\partial T} \boldsymbol{L} + E_s^{-1} \frac{\partial \nu}{\partial T} \boldsymbol{L}_0 \right) \boldsymbol{\sigma}_s + \boldsymbol{\alpha}_{\text{lin}} \tag{44}$$

The analogous expression for $\boldsymbol{\theta}_m$ [Eq. (27)] is then

$$\boldsymbol{\theta}_m = \left(-E_m^{-2} \frac{\partial E_m}{\partial T} \boldsymbol{L} + E_m^{-1} \frac{\partial \nu}{\partial T} \boldsymbol{L}_0 \right) \boldsymbol{\sigma}_m + \boldsymbol{\alpha}_{\text{lin}} \tag{45}$$

To use Eqs. (44) and (45) in practice, it is necessary to express $\boldsymbol{\sigma}_s$ and $\boldsymbol{\sigma}_m$ in terms of the stress and strain rates $\dot{\boldsymbol{\sigma}}$ and $\dot{\boldsymbol{\varepsilon}}$ and the thermal strain rate $\dot{\boldsymbol{\varepsilon}}_T$. This can be accomplished as follows.

The stresses in the viscous damper satisfy

$$\boldsymbol{\sigma}_m = \boldsymbol{C}_\eta \dot{\boldsymbol{\varepsilon}}_\eta \tag{46}$$

On the other hand, the modified viscous strain rates can be obtained from Eq. (36) as

$$\dot{\hat{\boldsymbol{\varepsilon}}}_\eta = -\boldsymbol{C}_E^{-1} \dot{\boldsymbol{\sigma}} + \dot{\boldsymbol{\varepsilon}} - \dot{\boldsymbol{\varepsilon}}_T \tag{47}$$

When Eqs. (29) and (37) are used, $\boldsymbol{\sigma}_m$ and $\boldsymbol{\sigma}_s$ can be expressed as

$$\boldsymbol{\sigma}_m = (E/E_m) \boldsymbol{C}_\eta \dot{\hat{\boldsymbol{\varepsilon}}}_\eta \tag{48}$$

$$\boldsymbol{\sigma}_s = \boldsymbol{\sigma} - \boldsymbol{\sigma}_m \tag{49}$$

For consistency, it is also assumed that [see Eq. (35)]

$$\boldsymbol{C}_\eta \equiv \eta \boldsymbol{N} \tag{50}$$

IV. Integration of the Constitutive Relationships

The constitutive relationship (36) can be interpreted as an ordinary differential equation that can be integrated to obtain either $\boldsymbol{\sigma}$ or $\boldsymbol{\varepsilon}$. The procedure will be illustrated for the case of integration to obtain $\boldsymbol{\sigma}$. This of course corresponds to a strain-driven problem in which the strain rate $\dot{\boldsymbol{\varepsilon}}$ and the rate of change of the temperature $\dot{T}$ are assumed known. The simplest way to integrate Eq. (36) is to use a forward Euler scheme. In this case, once the stress is known at time t, the corresponding stress at time $t + \Delta t$ can be found as

$$\boldsymbol{\sigma}(t + \Delta t) \approx \boldsymbol{\sigma}(t) + \boldsymbol{C}_E (\dot{\boldsymbol{\varepsilon}} - \dot{\hat{\boldsymbol{\varepsilon}}}_\eta - \dot{\boldsymbol{\varepsilon}}_T) \Delta t \tag{51}$$

A slightly more accurate way of integrating Eq. (36) numerically consists of finding an analytical solution first and then carrying out the numerical approximation. To this end, one uses Eqs. (48) and (37) to rewrite Eq. (36) as

$$\dot{\boldsymbol{\sigma}} = \boldsymbol{C}_E \dot{\boldsymbol{\varepsilon}} - \boldsymbol{C}_m \boldsymbol{C}_\eta^{-1} \boldsymbol{\sigma}_m - \boldsymbol{C}_E \hat{\boldsymbol{\alpha}} \dot{T} \tag{52}$$

When use is made of relations (29) and (37), one can write

$$\dot{\boldsymbol{\sigma}} = \boldsymbol{C}_E \dot{\boldsymbol{\varepsilon}} - (E_m/\eta)(\boldsymbol{\sigma} - \boldsymbol{\sigma}_s) - \boldsymbol{C}_E \hat{\boldsymbol{\alpha}} \dot{T} \tag{53}$$

which can be reordered to yield

$$\dot{\boldsymbol{\sigma}} + (E_m/\eta)\boldsymbol{\sigma} = \boldsymbol{C}_E \dot{\boldsymbol{\varepsilon}} + (E_m/\eta)\boldsymbol{\sigma}_s - \boldsymbol{C}_E \hat{\boldsymbol{\alpha}} \dot{T} \tag{54}$$

whose solution is

$$\boldsymbol{\sigma}(t) = \exp\left(-\frac{E_m}{\eta} t \right) \times \left[\int_0^t \exp\left(\frac{E_m}{\eta} \tau \right) \left(\boldsymbol{C}_E \dot{\boldsymbol{\varepsilon}} + \frac{E_m}{\eta} \boldsymbol{\sigma}_s - \boldsymbol{C}_E \hat{\boldsymbol{\alpha}} \dot{T} \right) \mathrm{d}\tau \right] \tag{55}$$

After some algebraic manipulations, an approximate incremental version of Eq. (55) is found as

$$\boldsymbol{\sigma}(t + \Delta t) \approx \exp[-(E_m/\eta)\Delta t]\boldsymbol{\sigma}(t) + \exp[-(E_m/\eta)(\Delta t/2)] \times [\boldsymbol{C}_E (\dot{\boldsymbol{\varepsilon}} - \hat{\boldsymbol{\alpha}} \dot{T}) + (E_m/\eta)\boldsymbol{\sigma}_s]_{t + \Delta t/2} \Delta t \tag{56}$$

where use has been made of the mean value theorem to estimate the second term.

For the isothermal case, Eq. (55) becomes

$$\dot{\boldsymbol{\sigma}} + (E_m/\eta)\boldsymbol{\sigma} = \boldsymbol{C}_E \dot{\boldsymbol{\varepsilon}} + (E_m/\eta)\boldsymbol{C}_s \boldsymbol{\varepsilon} \tag{57}$$

Equation (57) can be solved for $\boldsymbol{\sigma}$ and $\boldsymbol{\varepsilon}$ to obtain

$$\boldsymbol{\sigma}(t) = \exp\left(-\frac{E_m}{\eta} t \right) \times \left[\int_0^t \exp\left(\frac{E_m}{\eta} \tau \right) \left(\boldsymbol{C}_E \dot{\boldsymbol{\varepsilon}} + \frac{E_m}{\eta} \boldsymbol{C}_s \boldsymbol{\varepsilon} \right) \mathrm{d}\tau \right] \tag{58}$$

$$\boldsymbol{\varepsilon}(t) = \exp\left(-\frac{E_m E_s}{E\eta} t \right) \times \left[\int_0^t \exp\left(\frac{E_m E_s}{E\eta} \tau \right) \left(\boldsymbol{C}_E^{-1} \dot{\boldsymbol{\sigma}} + \frac{E_m}{\eta} \boldsymbol{C}_E^{-1} \boldsymbol{\sigma} \right) \mathrm{d}\tau \right] \tag{59}$$

respectively. From Eqs. (58) and (59), well-known relaxation and creep solutions for the present model can be readily obtained as[13]

$$\boldsymbol{G}(t) = \boldsymbol{C}_s + \boldsymbol{C}_m \exp[-(E_m/\eta)t] \tag{60}$$

$$\boldsymbol{J}(t) = \boldsymbol{C}_E^{-1} \exp[-(E_m E_s/\eta E)t] + \boldsymbol{C}_s^{-1}\{1 - \exp[-(E_m E_s/\eta E)t]\} \tag{61}$$

V. Incremental Solution Procedure

The objective of the present analysis is to find the viscoelastic response (represented, for example, by the effective creep compliance) of the composite question. The numerical integration procedure is, therefore, carried out within the context of the GMC equations. In the common case of elastic fibers embedded in a viscoelastic matrix, the equations of Sec. IV apply to the viscoelastic phase only. The elastic phase is handled in the standard manner by means of the appropriate constitutive equation [Eq. (2) with $\boldsymbol{\varepsilon}^*$ equal to zero]. As mentioned in Sec. IV, the integration of the constitutive equations for the viscoelastic phase can be accomplished either by using a simple forward Euler scheme or the slightly more accurate stepping approach based on the analytical solution [Eq. (54)]. Both approaches were tested numerically during the present study, but only the results obtained with the latter are presented. The numerical solution procedure is arranged so that it is strain and temperature driven, that is, the total effective strain rate $\dot{\bar{\boldsymbol{\varepsilon}}}$ and the rate of change of the temperature $\dot{T}$ are assumed known at each time step. For the creep compliance results presented in Sec. VII, an arbitrary stress step is first applied to the composite, and the corresponding strains are then calculated using the undotted version of Eq. (47). The process can then be applied as if the problem were strain driven. The details of the procedure are best appreciated if arranged in the form of an algorithm as shown in the following section. Only the steps corresponding to the viscoelastic phase are indicated. The elastic phase is treated in the standard manner. The index k indicates the time step.

The algorithm is as follows:

1) Obtain the matrices $\boldsymbol{A}_s$ and $\boldsymbol{A}_s^I$ [Eqs. (10) and (11)], and compute the effective stiffness matrix for the composite using Eq. (15).

2) Initialize all relevant variables, that is, set $k = 0$, $t = 0$, $T = T_0$, $\boldsymbol{\varepsilon}_{Nk} = \boldsymbol{0}$, $\boldsymbol{\sigma}_{Nk} = \boldsymbol{0}$, $\boldsymbol{\varepsilon}_{NTk} = \boldsymbol{0}$, $\boldsymbol{\varepsilon}_{sNTk} = \boldsymbol{0}$, $\hat{\boldsymbol{\varepsilon}}_{N\eta k} = \boldsymbol{0}$, and $\dot{\boldsymbol{\varepsilon}}_{NTk} = \boldsymbol{0}$. Here, $\dot{\bar{\boldsymbol{\varepsilon}}}_k$ and $\dot{T}_k$ are assumed known.

3) Find the strain rates in the subcells as [Eq. (9)]

$$\dot{\boldsymbol{\varepsilon}}_{Nk} = \boldsymbol{A}_s \dot{\bar{\boldsymbol{\varepsilon}}}_k + \boldsymbol{A}_s^I \dot{\hat{\boldsymbol{\varepsilon}}}_{N\eta k} + \boldsymbol{A}_s^I \dot{\boldsymbol{\varepsilon}}_{NTk}$$

4) Find the individual strains in the subcells as

$$\boldsymbol{\varepsilon}_{Nk+1} = \boldsymbol{\varepsilon}_{Nk} + \dot{\boldsymbol{\varepsilon}}_{Nk} \Delta t$$

5) For all subcells $(\beta\gamma)$ use the following steps:

a) Find $\boldsymbol{\sigma}_{sk}^{(\beta\gamma)}$, $\boldsymbol{\sigma}_{mk}^{(\beta\gamma)}$ [Eqs. (30) and (31)], and $\boldsymbol{\sigma}_{sk+1/2}^{(\beta\gamma)}$ as

$$\boldsymbol{\sigma}_{sk}^{(\beta\gamma)} = \boldsymbol{C}_s^{(\beta\gamma)}\left(\boldsymbol{\varepsilon}_k^{(\beta\gamma)} - \boldsymbol{\varepsilon}_{sTk}^{(\beta\gamma)}\right), \qquad \boldsymbol{\sigma}_{mk}^{(\beta\gamma)} = \boldsymbol{\sigma}_k^{(\beta\gamma)} - \boldsymbol{\sigma}_{sk}^{(\beta\gamma)}$$

$$\boldsymbol{\sigma}_{sk+\frac{1}{2}}^{(\beta\gamma)} = \boldsymbol{C}_s^{(\beta\gamma)}\left(\boldsymbol{\varepsilon}_{k+\frac{1}{2}}^{(\beta\gamma)} - \boldsymbol{\varepsilon}_{sTk+\frac{1}{2}}^{(\beta\gamma)}\right)$$

b) Find the viscous strain rate [Eq. (48)]:

$$\dot{\hat{\boldsymbol{\varepsilon}}}_{\eta k}^{(\beta\gamma)} = \left(E_m^{(\beta\gamma)}/E^{(\beta\gamma)}\right)\left(\boldsymbol{C}_{\eta k}^{(\beta\gamma)}\right)^{-1}\boldsymbol{\sigma}_{mk}^{(\beta\gamma)}$$

c) Find a modified stress rate as [Eq. (56)]

$$\dot{\hat{\boldsymbol{\sigma}}}_{k+\frac{1}{2}}^{(\beta\gamma)} = \boldsymbol{C}_E^{(\beta\gamma)}\left(\dot{\boldsymbol{\varepsilon}}_{k+\frac{1}{2}}^{(\beta\gamma)} - \dot{\boldsymbol{\varepsilon}}_{Tk+\frac{1}{2}}^{(\beta\gamma)}\right) + \left(E_m^{(\beta\gamma)}/\eta^{(\beta\gamma)}\right)\boldsymbol{\sigma}_{sk+\frac{1}{2}}^{(\beta\gamma)}$$

d) Find the new stress as [Eq. (56)]

$$\boldsymbol{\sigma}_{k+1}^{(\beta\gamma)} = \exp\left\{-\left[E_m^{(\beta\gamma)}/\eta^{(\beta\gamma)}\right]\Delta t\right\}\boldsymbol{\sigma}_k^{(\beta\gamma)} + \exp\left\{-\left[E_m^{(\beta\gamma)}/\eta^{(\beta\gamma)}\right](\Delta t/2)\right\}\hat{\boldsymbol{\sigma}}_{k+\frac{1}{2}}^{(\beta\gamma)}\Delta t$$

e) Calculate $\boldsymbol{\theta}_s^{(\beta\gamma)}$ and $\boldsymbol{\theta}_m^{(\beta\gamma)}$ using Eqs. (26) and (27).

f) Calculate $\hat{\boldsymbol{\alpha}}^{(\beta\gamma)}$ from Eq. (39) and the new thermal strain rate as $\dot{\boldsymbol{\varepsilon}}_{Tk+1}^{(\beta\gamma)} = \hat{\boldsymbol{\alpha}}^{(\beta\gamma)}\dot{T}_k$.

g) Calculate the new thermal strain:

$$\boldsymbol{\varepsilon}_{Tk+1}^{(\beta\gamma)} = \boldsymbol{\varepsilon}_{Tk}^{(\beta\gamma)} + \dot{\boldsymbol{\varepsilon}}_{Tk+1}^{(\beta\gamma)}\Delta t$$

h) Update the thermal strain in the isolated spring element:

$$\boldsymbol{\varepsilon}_{sTk}^{(\beta\gamma)} = \boldsymbol{\varepsilon}_{sTk}^{(\beta\gamma)} + \boldsymbol{\theta}_s^{(\beta\gamma)}\dot{T}_k\Delta t$$

i) Calculate the new viscous strain [Eq. (47)]:

$$\hat{\boldsymbol{\varepsilon}}_{\eta k}^{(\beta\gamma)} = -\left(\boldsymbol{C}_E^{(\beta\gamma)}\right)^{-1}\boldsymbol{\sigma}_{k+1}^{(\beta\gamma)} + \boldsymbol{\varepsilon}_{k+1}^{(\beta\gamma)} - \boldsymbol{\varepsilon}_{Tk}^{(\beta\gamma)}$$

6) Set $\boldsymbol{\varepsilon}_{Nk} = \boldsymbol{\varepsilon}_{Nk+1}$, $\boldsymbol{\sigma}_{Nk} = \boldsymbol{\sigma}_{Nk+1}$, $\hat{\boldsymbol{\varepsilon}}_{N\eta k} = \hat{\boldsymbol{\varepsilon}}_{N\eta k+1}$, and $\hat{\boldsymbol{\varepsilon}}_{NTk} = \hat{\boldsymbol{\varepsilon}}_{NTk+1}$.

7) Find the effective viscous and thermal strains $\bar{\hat{\boldsymbol{\varepsilon}}}_\eta$ and $\bar{\boldsymbol{\varepsilon}}_T$ by means of Eqs. (17) and (18) and integrate $\bar{\dot{\boldsymbol{\varepsilon}}}_k$ to get $\bar{\boldsymbol{\varepsilon}}_k$.

8) Find the effective stress $\bar{\boldsymbol{\sigma}}$ from Eq. (14).

9) If $k <$ maximum number of load steps, then set $t = t + \Delta t$, $k = k + 1$, and go to step 3, otherwise stop.

The notation $k + \frac{1}{2}$ has been used to represent quantities evaluated at time $t + \Delta t/2$ [Eq. (56)]. These quantities are approximated as the average at time step k and $k + 1$.

In case the plain forward Euler procedure is preferred, steps c and d should be replaced by the following steps:

c) Find the stress rate [Eqn. (18)]: $\dot{\boldsymbol{\sigma}}_k^{(\beta\gamma)} = \boldsymbol{C}_E^{(\beta\gamma)}(\dot{\boldsymbol{\varepsilon}}_k^{(\beta\gamma)} - \dot{\hat{\boldsymbol{\varepsilon}}}_{\eta k}^{(\beta\gamma)} - \dot{\boldsymbol{\varepsilon}}_{Tk}^{(\beta\gamma)})$.

d) Integrate the stress rate: $\boldsymbol{\sigma}_{k+1}^{(\beta\gamma)} = \boldsymbol{\sigma}_k^{(\beta\gamma)} + \dot{\boldsymbol{\sigma}}_k^{(\beta\gamma)}\Delta t$.

VI. Computational Aspects

One of the difficulties of using GMC for other than elastic problems is the size of the matrices involved in the calculations. Therefore, it is important to store and factor the matrix $\boldsymbol{A}$ in Eqs. (10) and (11) sparsely. The matrices $\boldsymbol{A}_s$ and $\boldsymbol{A}_s^I$ must usually be stored as fully populated matrices [Eqs. (10) and (11)]. For the problem of finding the effective elastic properties of a composite, only $\boldsymbol{A}_s$ needs to be calculated. This matrix is a $6N_\beta N_\gamma \times 6$ matrix and can usually be stored completely, while still permitting the solution of problems with a large number of subcells.[6] For inelastic problems, however, storage of $\boldsymbol{A}_s^I$ as a fully populated matrix is prohibitive. $\boldsymbol{A}_s^I$ is a $6N_\beta N_\gamma \times 6N_\beta N_\gamma$ matrix, and to store it completely for a problem with 2500 subcells would require 1.8 GB of memory (using double precision). To perform analyses that require high-resolution subcell models, it is necessary to reduce the storage requirements imposed by $\boldsymbol{A}_s^I$. This has been accomplished in Ref. 4 by means of a reformulation of the GMC equations. This reduces considerably the computational and storage requirements of the method. Alternatively, for some nonlinear problems, storage of $\boldsymbol{A}_s^I$ can be avoided altogether. This has been done in Ref. 7 by means of a tangent stiffness matrix formulation for plasticity problems . In this study, we present yet a third approach. It also avoids complete storage of $\boldsymbol{A}_s^I$. This approach is described next.

Equation (9) is rewritten as

$$\boldsymbol{\varepsilon}_N = \boldsymbol{A}_s\bar{\boldsymbol{\varepsilon}} + \boldsymbol{A}^{-1}\left(\boldsymbol{A}^I\hat{\boldsymbol{\varepsilon}}_{N\eta}\right) + \boldsymbol{A}^{-1}\left(\boldsymbol{A}^I\boldsymbol{\varepsilon}_{NT}\right) \tag{62}$$

If instead of Eq. (57), Eq. (67) is used to calculate the strains in the subcells, it is not necessary to generate and store $\boldsymbol{A}_s^I$. Instead, $\boldsymbol{A}$ is factored once, and then, at each load step, $\boldsymbol{A}^I$ (which is also stored sparsely) is multiplied by the current value of the viscous and thermal strains $\hat{\boldsymbol{\varepsilon}}_{N\eta}$ and $\boldsymbol{\varepsilon}_{NT}$. In this way, the entire process requires only one factorization of $\boldsymbol{A}$ at the beginning of the procedure and two triangular solves at each load step. The procedure allows for the solution of problems with a large number of subcells. A problem with 10,000 subcells and 60 time steps similar to the ones shown subsequently takes about 12 h of CPU time on an SGI Indigo2 workstation.

VII. Numerical Results

The hereditary viscoelastic model utilized in the present study has been found useful in modeling the behavior of a titanium alloy (TIMETAL 21S) at a wide range of temperatures.[10,14] The corresponding numerical approach developed here is used to analyze graphite/epoxy unidirectional composites with various fiber arrangements and fiber shapes. The three-element hereditary viscoelastic model can be calibrated to fit experimental results of real viscoelastic polymeric materials. This has been done, for instance, for the 934 epoxy resin of Ref. 8. This epoxy resin, however, exhibits relatively little viscoelasticity. To better examine the influence of fiber shape and fiber arrangement on the viscoelastic response of composite materials, a hypothetical viscoelastic material (epoxy-h) was used as the matrix material in the numerical experiments of the present study. T300 graphite fibers with real properties[3] were used as reinforcement material.

Two sets of numerical experiments were performed. In the first set, the influence of fiber arrangement and fiber shape on the isothermal response of composites was studied. Four different fiber arrangements and three different fiber shapes were considered. These are shown in Figs. 3 and 4. In the second set, the response of the composite to thermal load at different heating rates was examined.

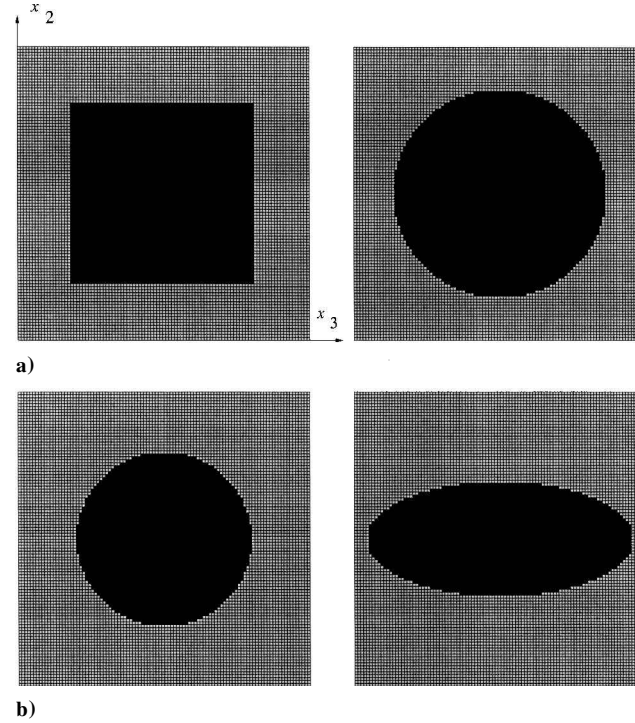

Fig. 3 Microstructures with different fiber shapes, 10,000 subcells; fiber volume fractions: a) 0.4 and b) 0.28.

Table 1 Mechanical properties of materials used in numerical experiments

Property[a]	T300 graphite fibers at 22°C	T300 graphite fibers at 121°C	Epoxy-h at 22°C	Epoxy-h at 121°C
E_A, MPa	202,820	214,330	——	——
E_T, MPa	25,300	14,820	——	——
G_A, MPa	44,112	68,180	——	——
ν	0.443	0.450	0.300	0.306
α_A, °C^{-1}	1.33×10^{-6}	-1.33×10^{-6}	3.0×10^{-4}	3.0×10^{-4}
α_T, °C^{-1}	7.04×10^{-6}	7.04×10^{-6}	3.0×10^{-4}	3.0×10^{-4}
E_s, MPa	——	——	4,000	2,735
E_m, MPa	——	——	3,000	4,895
η, MPa · s	——	——	2.5×10^6	2.27×10^6

[a]Subscript A indicates axial and subscript T indicates transverse.

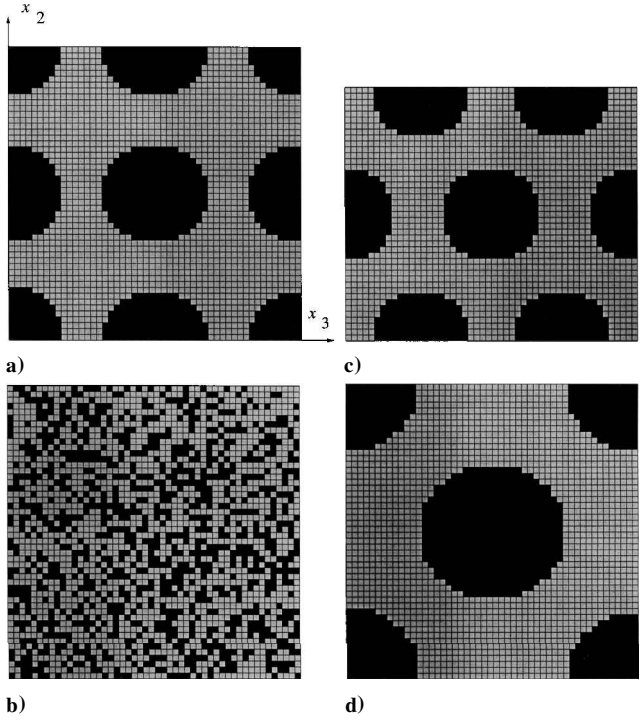

Fig. 4 Fiber volume fraction 0.4, 2500 subcells (2150 for the hexagonal packing): a) square-edge packing of circular fibers, b) randomly distributed fiber material, c) hexagonal (triangular) packing of circular fibers, and d) square-diagonal packing of circular fibers.

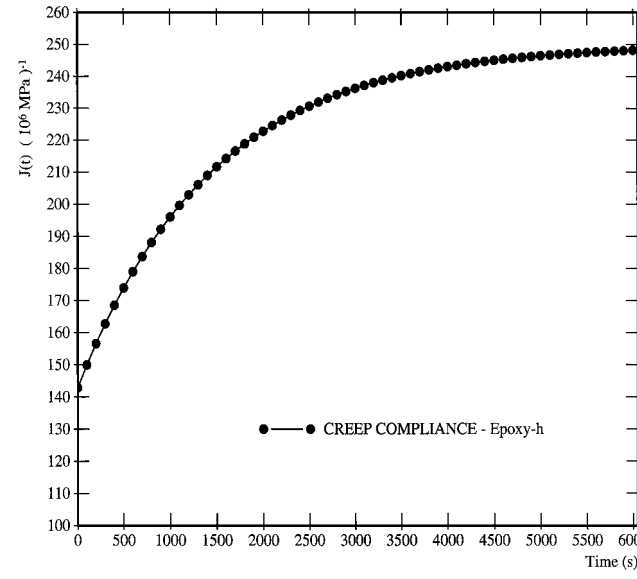

Fig. 5 Creep compliance of hypothetical epoxy (epoxy-h); thermomechanical properties shown in Table 1.

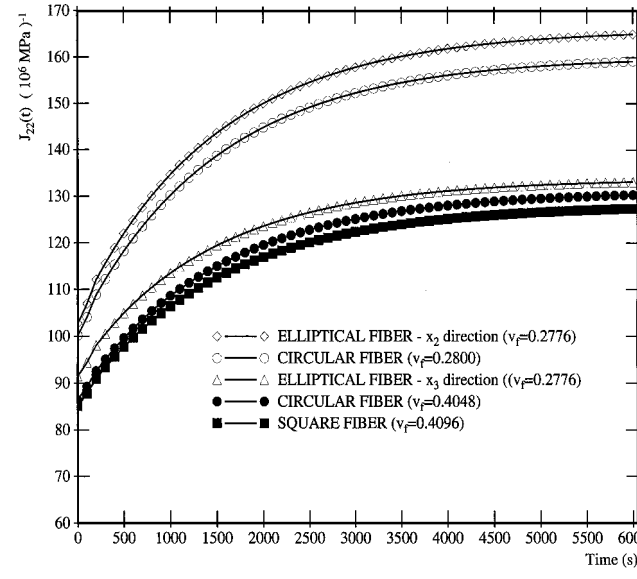

Fig. 6 Transverse creep compliances ($\varepsilon_{22}/\sigma_{22}$) corresponding to composite microstructures with different fiber shapes (Fig. 3).

The properties of the materials used are listed in Table 1. The creep compliance function [Eq. (61)] corresponding to the hypothetical epoxy is shown in Fig. 5. The parameters of the three-element standard solid model used to produce Fig. 5 are also listed in Table 1.

A. Influence of Fiber Shape and Fiber Arrangement: Isothermal Case

Figure 6 shows the responses (transverse creep compliances) corresponding to the microstructures shown in Fig. 3. These microstructures differ only in fiber shape. To capture the effect of fiber shape better, high-resolution models (10,000 subcells) were used to generate these responses. Note that there is a small but noticeable difference in the responses of the elliptic and circular fibers when the loading direction is the x_2 direction (about 3.7% at the end of the loading cycle). When the direction of loading is the x_3 direction, the elliptical fiber response is 16% lower than that of the circular fiber. The reason for this is that the elliptical fiber has its larger semi-axis directed in the x_3 direction. Very little difference in the response is exhibited by the circular and square fiber microstructures. This is in contrast to what has been observed in Refs. 7, 15, and 16 for plastic behavior. The reason is that fiber shape and fiber arrangement have a significant effect on the magnitude of the hydrostatic component of the stress. In plasticity models, this hydrostatic component plays an important role because it inhibits the progression of the plastic zone in the matrix. In contrast, the present viscoelastic model makes no attempt to distinguish between viscoelastic effects due to hydrostatic and deviatoric components of the stress.

The creep compliance functions corresponding to the different microstructure architectures of Fig. 4 are shown in Fig. 7. The first observation is that all microstructures are more compliant in longitudinal shear than in transverse tension. The responses corresponding to the hexagonal and random microstructures almost coincide for the longitudinal shear compliance and are very close to each other for the transverse compliance. This is because a hexagonal microstructure exhibits an almost perfect transversely isotropic behavior just as a random microstructure does.[6] The responses corresponding to the square-edge and the single circular fiber should theoretically coincide because they are indeed the same microstructure. The small differences seen in Fig. 7 for these two cases are due to the modeling of the microstructures. (Because arrays of 50×50 subcells were used, the circular fiber shape is more accurately modeled for the single fiber than for the square-edge array.) There are significant differences between the responses corresponding to the square-edge, the hexagonal and random, and the square-diagonal architectures. The differences in response for the circular fiber and the random microstructure are of the order of 14% at the end of the loading

Table 2 Initial mechanical properties corresponding to microstructures shown in Figs. 3 and 4

Microstructure	Property, MPa								
	E_{11}	E_{22}	E_{33}	ν_{23}	ν_{13}	ν_{12}	G_{23}	G_{13}	G_{12}
Elliptical, $v_f = 0.28$	61,398	9,733	10,933	0.357	0.362	0.331	3,333	5,860	3,715
Circular, $v_f = 0.28$	61,853	9,983	10,016	0.387	0.344	0.344	3,340	4,102	4,061
Circular, $v_f = 0.40$	85,359	11,462	11,602	0.381	0.364	0.362	3,725	5,280	5,068
Square edge, $v_f = 0.40$	82,226	11,201	11,446	0.380	0.363	0.358	3,668	5,198	4,836
Hexagonal, $v_f = 0.40$	85,707	10,737	11,214	0.394	0.366	0.355	3,731	4,975	4,397
Random, $v_f = 0.40$	85,330	10,584	10,601	0.412	0.358	0.357	3,725	4,372	4,351
Square diagonal, $v_f = 0.40$	75,562	10,207	10,289	0.406	0.353	0.351	3,571	4,206	4,117

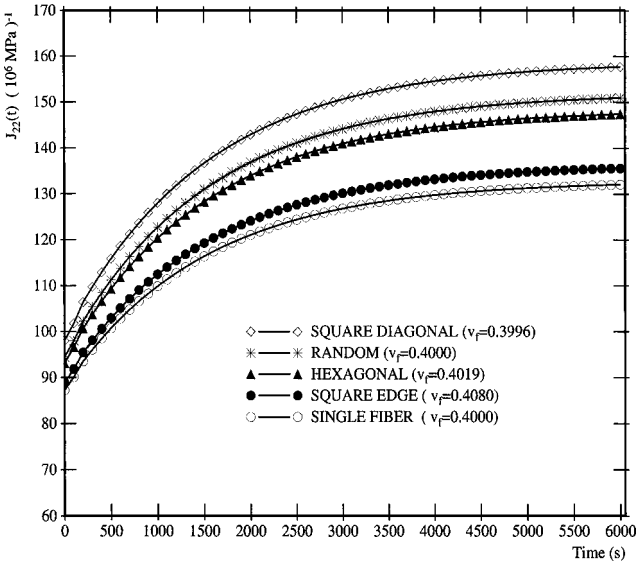

Transverse ($\varepsilon_{22}/\sigma_{22}$) creep compliances

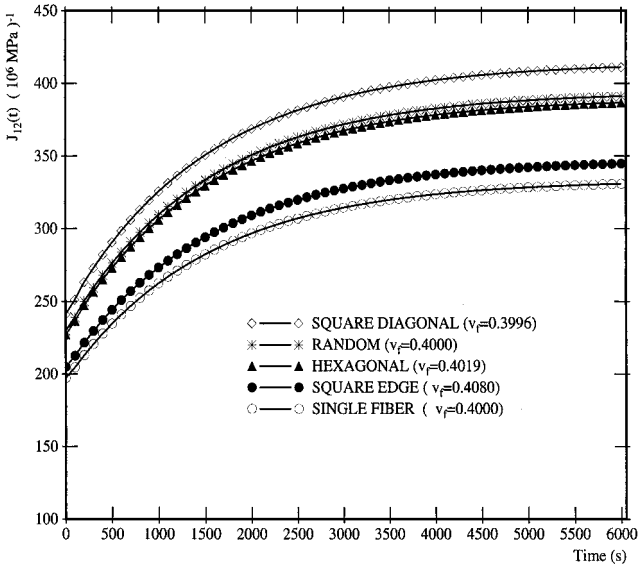

Longitudinal shear ($2\varepsilon_{12}/\sigma_{12}$) creep compliances

Fig. 7 Creep compliances corresponding to composite microstructures with different architectures (Fig. 4).

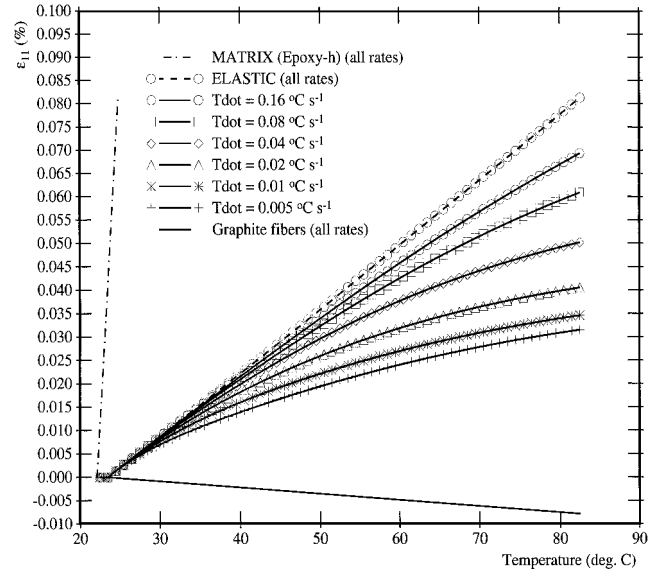

Fig. 8 Viscoelastic response of graphite–epoxy composite for thermal load at different heating rates; square-edge packing of T300 graphite circular fibers (Fig. 4), v_f = 0.4.

cycle for the transverse loading and of the order of 18% for longitudinal shear. The square-diagonal microstructure turns out to be the most compliant for both longitudinal shear and transverse normal loading. The square-diagonal microstructure is 19% more compliant (at the end of the loading cycle) than the single circular fiber for the transverse loading and 24% more compliant than the single circular fiber for longitudinal shear. This can be explained by that the square-diagonal microstructure is actually the square-edge microstructure rotated 45 deg. Note that part of the differences in response found in all of these cases can be explained by the differences in (initial) effective properties of the different microstructures (Table 2). A portion of the difference in responses, however, is due to viscoelastic effects. The influence of the fiber geometry on the creep times of the different composite microstructures is also indicated by the differences in the initial slopes of the creep compliance responses shown in Figs. 6 and 7.

B. Nonisothermal Case

The response of the composite to thermal load was examined for a series of different heating rates and for temperature-dependent properties. The properties are presented in Table 1. The properties for the T300 graphite fibers are actual experimental values taken from Refs. 3 and 8. The properties for the epoxy-h are hypothetical but chosen so that its behavior with temperature is analogous to that of the epoxy resin reported in Ref. 8. Six rates were utilized, namely, $\dot{T} = 0.005, 0.01, 0.02, 0.04, 0.08$, and $0.16^\circ\text{C s}^{-1}$. Results were obtained for the strain in the x_1 and x_2 directions. Very few viscoelastic effects were found for the strain in the x_2 direction. Therefore, only the results for the longitudinal strain are presented. Circular fibers corresponding to square-edge and hexagonal packing (Fig. 4) were utilized. Very little difference in the response was found for different packing arrangements and/or fiber shapes. As a consequence, results are presented only for the square-edge packing. These are shown in Fig. 8. Results show a difference of 160% in the final strains between the slower ($\dot{T} = 0.005^\circ\text{C s}^{-1}$) and the faster ($\dot{T} = 0.16^\circ\text{C s}^{-1}$) rate. This difference is of course a function of the viscoelastic properties of the matrix, as well as the mismatch in the coefficients of thermal expansion between fiber and matrix.

C. Numerical Accuracy of the Results

All results presented in the present study were obtained using double precision on an SGI Indigo2 workstation. There is very little error

in the numerical integration procedure utilized. When, for instance, Fig. 5 is referred to, the asymptotic value of the creep compliance is about 250^{-6} MPa^{-1}, which is exactly the inverse of 4000 MPa, the E_s value given in row five, column two of Table 2 for epoxy-h.

VIII. Summary

A computationally efficient viscoelastic formulation of GMC has been presented and used to study the behavior of complex microstructure unidirectional composites with viscoelastic matrices. A multi-axial hereditary viscoelastic model developed in Ref. 10 was used as the theoretical framework of the formulation. The viscoelastic creep responses of composites with different fiber shapes and fiber arrangements were analyzed and compared. High-resolution cell models (with up to 10,000 subcells) of the composites were used for the fiber-shape comparison cases. It was found that differences in viscoelastic response due to differences in fiber shape are not significant (about 3.7% for the case of elliptical vs circular fibers). However, significant differences are found for composites with different fiber arrangements. These differences can be on the order of 24%. Experimental research is necessary to verify some of the results of the present study. On the other hand, the results seem to confirm what has been observed in similar numerical studies for plastic and viscoplastic behavior of composites. It is believed that the numerical capability developed is an efficient tool to predict the viscoelastic behavior of complex microstructure multiphase composites. Furthermore, the capability can be used within structural analysis codes as a constitutive model subroutine, just as has been done with the commercial code Hipersizer.

Appendix: Derivation of the Constitutive Equation for a Parallel Multi-Element Maxwell Model

For the ith Maxwell element in Fig. 1b, we have

$$\dot{\boldsymbol{\sigma}}_i = \boldsymbol{C}_i(\dot{\boldsymbol{\varepsilon}} - \dot{\boldsymbol{\varepsilon}}_{i\eta} - \dot{\boldsymbol{\varepsilon}}_{iT}) \tag{A1}$$

where $\dot{\boldsymbol{\varepsilon}}$ is the total strain rate, $\dot{\boldsymbol{\varepsilon}}_{i\eta}$ is the strain rate in the dashpot, $\dot{\boldsymbol{\varepsilon}}_{iT}$ is the thermal strain rate, $\boldsymbol{C}_i$ the material stiffness matrix, and $\dot{\boldsymbol{\sigma}}_i$ is the stress rate. Because the Maxwell elements in Fig. 1b are connected in parallel, the total stress rate is

$$\dot{\boldsymbol{\sigma}} = \sum_i \boldsymbol{C}_i(\dot{\boldsymbol{\varepsilon}} - \dot{\boldsymbol{\varepsilon}}_{i\eta} - \dot{\boldsymbol{\varepsilon}}_{iT}) \tag{A2}$$

which can be written

$$\dot{\boldsymbol{\sigma}}_i = \boldsymbol{C}\left[\dot{\boldsymbol{\varepsilon}} - \boldsymbol{C}^{-1}\sum_i(\boldsymbol{C}_i\dot{\boldsymbol{\varepsilon}}_{i\eta}) - \boldsymbol{C}^{-1}\sum_i(\boldsymbol{C}_i\dot{\boldsymbol{\varepsilon}}_{iT})\right] \tag{A3}$$

where

$$\boldsymbol{C} = \sum_i(\boldsymbol{C}_i) \tag{A4}$$

Equation (A3) can be written as

$$\dot{\boldsymbol{\sigma}} = \boldsymbol{C}(\dot{\boldsymbol{\varepsilon}} - \dot{\hat{\boldsymbol{\varepsilon}}}_\eta - \dot{\boldsymbol{\varepsilon}}_T) \tag{A5}$$

provided that

$$\dot{\hat{\boldsymbol{\varepsilon}}}_\eta \equiv \boldsymbol{C}^{-1}\sum_i(\boldsymbol{C}_i\dot{\boldsymbol{\varepsilon}}_{i\eta}) \tag{A6}$$

$$\dot{\boldsymbol{\varepsilon}}_T \equiv \boldsymbol{C}^{-1}\sum_i(\boldsymbol{C}_i\dot{\boldsymbol{\varepsilon}}_{iT}) \tag{A7}$$

Equation (A5) is formally the same as Eq. (36), which is the basis for the implementation of a viscoelastic model into GMC. On the other hand, at least in theory, it is possible to model real viscoelastic materials to any desired degree of accuracy using multi-element Maxwell models in parallel.[13] Therefore, it is possible to apply the methodology developed in the present paper to the analysis of composites with realistic viscoelastic matrix materials.

Acknowledgments

This work was supported by the Collier Research and Development Co. under Contract CRC-97-01. The Collier Research and Development Co. was in turn supported by the NASA John H. Glenn Research Center at Lewis Field under Contract NRA-96-LeRC-1. Their support is greatly appreciated.

References

[1]Paley, M., and Aboudi, J., "Micromechanical Analysis of Composites by the Generalized Methods of Cells," *Mechanics of Materials*, Vol. 14, No. 1, 1992, pp. 127–139.

[2]Aboudi, J., "Micromechanical Analysis of Composites by the Method of Cells—Update," *Applied Mechanics Reviews*, Vol. 49, No. 10, 1996, pp. S83–S91.

[3]Aboudi, J., *Mechanics of Composite Materials—A Unified Micromechanical Approach*, Elsevier, Amsterdam, 1991, Chap. 4.

[4]Pindera, M.-J., and Bednarcyk, B. A., "An Efficient Formulation of the Generalized Method of Cells for Unidirectional, Multi-Phase Composites with Complex Microstructures," *Composites Part B: Engineering*, Vol. 30, No. 1, 1999, pp. 87–105.

[5]Arnold, S. M., Bednarcyk, B. A., Wilt, T. E., and Trowbridge, D., "Micromechanics Analysis Code with the Generalized Method of Cells Model (MAC/GMC)," NASA TM-1999-209070, 1999.

[6]Orozco, C. E., "Computational Aspects of Modeling Complex Microstructure Composites Using GMC," *Composites Part B: Engineering*, Vol. 28, No. 1–2, 1997, pp. 167–175.

[7]Orozco, C. E., and Pindera, M.-J., "Plastic Analysis of Complex Microstructure Composites Using Generalized Method of Cells," *AIAA Journal*, Vol. 37, No. 4, 1999, pp. 482–488.

[8]Yancey, R. N., and Pindera, M.-J., "Micromechanical Analysis of the Creep Response of Unidirectional Composites," *Journal of Engineering Materials and Technology*, Vol. 112, No. 2, 1990, pp. 157–163.

[9]Aboudi, J., "Micromechanical Modeling of Finite Viscoelastic Multiphase Composites," *Zeitschrift für Angewandte Mathematik und Physik*, Vol. 51, No. 1, 2000, pp. 114–134.

[10]Saleeb, A. F., and Arnold, S. M., "A General Reversible Hereditary Constitutive Model: Part I Theoretical Developments," NASA TM 107493, 1997.

[11]Hilton, H. H., "On the Inadmissibility of Separation of Variables Solutions in Linear Anisotropic Viscoelasticity," *Mechanics of Composite Materials and Structures*, Vol. 3, No. 1, 1996, pp. 97–100.

[12]Hilton, H. H., and Yi, S., "The Significance of Anisotropic Viscoelastic Poisson Ratio Stress and Time Dependencies," *Journal of Solids and Structures*, Vol. 35, No. 23, 1998, pp. 3081–3095.

[13]Findley, W. N., Lai, J. S., and Onaran, K., *Creep and Relaxation of Nonlinear Viscoelastic Materials*, Dover, New York, 1976, Chap. 5.

[14]Arnold, S. M., Saleeb, A. F., and Castelli, M. G., "A General Reversible Hereditary Constitutive Model: Part II Application to a Titanium Alloy," NASA TM 107494, 1997.

[15]Brockenbrough, J. R., and Suresh, S., "Plastic Deformation of Continuous Fiber-Reinforced Metal-Matrix Composites: Effects of Fiber Shape and Distribution," *Scripta Metallurgica et Materialia*, Vol. 24, No. 2, 1990, pp. 325–330.

[16]Brockenbrough, J. R., Suresh, S., and Wienecke, H. A., "Deformation of Metal-Matrix Composites with Continuous Fibers: Geometrical Effects of Fiber Distribution and Shape," *Scripta Metallurgica et Materialia*, Vol. 39, No. 5, 1991, pp. 735–752.

A. M. Waas
Associate Editor